HHS Public Access

Author manuscript

Nat Genet. Author manuscript; available in PMC 2015 July 01.

Published in final edited form as:

Nat Genet. 2014 July ; 46(7): 722–725. doi:10.1038/ng.2986.

Identification of recurrent *SMO* and *BRAF* mutations in ameloblastomas

Robert T Sweeney[1,12], **Andrew C McClary**[1,12], **Benjamin R Myers**[2,3,4,5,12], **Jewison Biscocho**[1,12], **Lila Neahring**[2,3,4,5], **Kevin A Kwei**[6,11], **Kunbin Qu**[6], **Xue Gong**[1], **Tony Ng**[7], **Carol D Jones**[1], **Sushama Varma**[1], **Justin I Odegaard**[1], **Toshihiro Sugiyama**[8], **Souichi Koyota**[8], **Brian P Rubin**[9], **Megan L Troxell**[10], **Robert J Pelham**[6], **James L Zehnder**[1], **Philip A Beachy**[2,3,4,5], **Jonathan R Pollack**[1], and **Robert B West**[1]

[1]Department of Pathology, Stanford University, Stanford, California, USA

[2]Department of Biochemistry, Stanford University, Stanford, California, USA

[3]Department of Developmental Biology, Stanford University, Stanford, California, USA

[4]Institute for Stem Cell Biology and Regenerative Medicine, Stanford University, Stanford, California, USA

[5]Howard Hughes Medical Institute, Stanford University School of Medicine, Stanford, California, USA

[6]Genomic Health, Redwood City, California, USA

[7]Department of Pathology and Laboratory Medicine, University of British Columbia, Vancouver, British Columbia, Canada

[8]Department of Biochemistry, Akita University Graduate School of Medicine, Akita, Japan

[9]Department of Anatomic Pathology, Cleveland Clinic, Cleveland, Ohio, USA

[10]Department of Pathology, Oregon Health and Sciences University, Portland, Oregon, USA

Abstract

Correspondence should be addressed to J.R.P. (pollack1@stanford.edu), P.A.B. (pbeachy@stanford.edu) or R.B.W. (rbwest@stanford.edu).

[11]Present address: Onyx Pharmaceuticals, South San Francisco, California, USA.

[12]These authors contributed equally to this work.

AUTHOR CONTRIBUTIONS

R.T.S., A.C.M., J.R.P. and R.B.W. designed the study and wrote the manuscript. A.C.M., B.R.M., J.R.P. and R.B.W. designed the figures. R.T.S., X.G., J.R.P. and R.B.W. analyzed raw sequence data. J.B. and J.R.P. performed mutation validation (PCR and Sanger sequencing). B.R.M., L.N., J.B., J.R.P. and P.A.B. designed and implemented functional studies. C.D.J., J.I.O. and J.L.Z. performed targeted sequencing (TruSeq). K.A.K., K.Q. and R.J.P. performed transcriptome sequencing. S.V. performed immunohistochemistry. T.N., B.P.R. and M.L.T. provided cases for evaluation. T.S. and S.K. provided key cell line reagents.

COMPETING FINANCIAL INTERESTS

The authors declare no competing financial interests.

Accession codes. Raw sequence reads are available in the database of Genotypes and Phenotypes (dbGaP) under accession phs000739.v1.p1.

Note: Any Supplementary Information and Source Data files are available in the online version of the paper.

Here we report the discovery of oncogenic mutations in the Hedgehog and mitogen-activated protein kinase (MAPK) pathways in over 80% of ameloblastomas, locally destructive odontogenic tumors of the jaw, by genomic analysis of archival material. Mutations in *SMO* (encoding Smoothened, SMO) are common in ameloblastomas of the maxilla, whereas *BRAF* mutations are predominant in tumors of the mandible. We show that a frequently occurring *SMO* alteration encoding p.Leu412Phe is an activating mutation and that its effect on Hedgehog-pathway activity can be inhibited by arsenic trioxide (ATO), an anti-leukemia drug approved by the US Food and Drug Administration (FDA) that is currently in clinical trials for its Hedgehog-inhibitory activity. In a similar manner, ameloblastoma cells harboring an activating *BRAF* mutation encoding p.Val600Glu are sensitive to the BRAF inhibitor vemurafenib. Our findings establish a new paradigm for the diagnostic classification and treatment of ameloblastomas.

Ameloblastoma, a locally destructive tumor, is thought to exhibit characteristics of ameloblastic differentiation[1]. Tumor cells resemble ameloblasts, cells in the developing tooth responsible for depositing enamel during tooth development (odontogenesis). Therapeutic options are few, and these tumors often require disfiguring wide local excision with high rates of recurrence. Research into the pathogenesis of ameloblastoma has largely been driven by clues derived from histological appearance and from normal tooth development. Rare tumor types such as ameloblastoma are not only understudied but are typically only accessible as formalin-fixed, paraffin-embedded (rather than freshly frozen) specimens that have been thought to be suboptimal for genomic analysis. Thus, relatively little genomic data have been generated on this tumor type. We have recently shown that transcriptome sequencing of formalin-fixed, paraffin-embedded specimens can effectively identify gene transcript fusions, suggesting that it might represent a more generally useful approach to study rare tumor genetics[2].

In a survey of rare neoplasia to discover driver mutations, we performed whole-transcriptome sequencing on formalin-fixed, paraffin-embedded material from two cases of ameloblastoma. This is an approach that may be efficient for the screening of rare neoplasia for clinically targetable, activating mutations, as these mutations are typically in well-expressed genes and thus easily detected in full-transcriptome libraries. Libraries of total RNA were prepared from rRNA-depleted RNA isolated from formalin-fixed, paraffin-embedded specimens. A custom analytical pipeline (Online Methods) identified high-confidence single-nucleotide variations (SNVs) but no gene fusions. Candidate SNVs were prioritized for further validation on the basis of their presence in both tumor samples and/or on the basis of previously known involvement of the identified gene or pathway in tooth bud development[3]. Candidate mutations were validated in an independent cohort consisting of 26 cases from 4 institutions (Supplementary Table 1), using targeted-capture deep sequencing and/or PCR with Sanger sequencing. Analysis of paired tumor-normal tissue in a subset of the validation cohort confirmed that the mutations were somatic.

From this analysis, we identified highly recurrent somatic mutations in two key developmental or growth factor signaling pathways—the Hedgehog and MAPK pathways. In all, 39% (11/28) of the tumors had mutations in *SMO* (an essential seven-transmembrane Hedgehog signal transduction component; 10 encoding p.Leu412Phe and 1 encoding

p.Trp535Leu) and 46% (13/28) had *BRAF* mutations (12 encoding p.Val600Glu and 1 encoding p.Leu597Arg) (Fig. 1a and Supplementary Fig. 1). *SMO* and *BRAF* mutations tended to be mutually exclusive ($P = 0.02$, two-sided Fisher's exact test), suggesting that these alterations might define two independent genetic etiologies for ameloblastoma. There was some correlation between mutation status and previously established morphological subtypes, as most (8/10) plexiform variants had a *SMO* mutation ($P < 0.02$), whereas most follicular and desmoplastic variants carried either *SMO* or *BRAF* mutation. Strikingly, *SMO* mutations exhibited a marked preponderance in maxillary ameloblastomas (9/11 cases) compared to mandibular cases (1/13) ($P < 0.001$), whereas *BRAF* mutations exhibited the reverse pattern, with a higher frequency in mandibular (9/13) compared to maxillary (1/11; encoding p.Leu597Arg) cases ($P = 0.01$) (Fig. 1b). Using available information on clinical outcome, we observed a trend toward earlier recurrence for tumors with *SMO* mutations (three of five *SMO* mutants versus one of six *BRAF* mutants recurred within 3 years after initial treatment; $P = 0.24$; Supplementary Table 1); analysis of a larger cohort is needed to substantiate this finding. Additional mutations in the MAPK pathway were also identified, including four cases (15%) with mutation of *KRAS* (encoding p.Gly12Arg) and five cases (19%) with mutation of *FGFR2* (four encoding p.Cys382Arg and one encoding p.Asn549Lys), the presumptive upstream receptor tyrosine kinase. In all but one case, mutation of *BRAF* was mutually exclusive with mutations in *KRAS* and *FGFR2* ($P < 0.05$). Expression of mutant BRAF protein, evaluated by immunohistochemistry for BRAF Val600Glu, was only seen in cases with confirmed presence of the corresponding mutation in *BRAF*, with some qualitative increase in expression at the leading edge of the epithelial cell component, adjacent to the stroma (Supplementary Fig. 2).

Previous studies have demonstrated that the recurring *BRAF*, *KRAS* and *FGFR2* mutations identified in this ameloblastoma cohort are activating mutations present in other cancers[4–6]. The *SMO* mutation encoding p.Trp535Leu, found in one case, is also known to be a frequent activating mutation in sporadic basal cell carcinoma[7]. The *SMO* mutation encoding p.Leu412Phe, the 'hotspot' *SMO* mutation in our study, was only recently reported in a subset of meningiomas[8]. To evaluate the functional consequences of the p.Leu412Phe alteration, we measured Hedgehog-pathway activation mediated by wild-type or mutant forms of SMO using a previously established Gli-driven luciferase reporter assay in $Smo^{-/-}$ mouse embryonic fibroblasts (MEFs) (Fig. 2)[9]. Of note, these fibroblasts also express basal levels of Ptch1, the 12-pass Hedgehog receptor that, in the absence of Hedgehog ligand, inhibits Smo. As expected, wild-type human SMO was essentially devoid of basal activity in this assay (resulting in <1% of the maximal Sonic Hedgehog (Shh)-induced response). In contrast, the Leu412Phe mutant showed substantially elevated, constitutive activity (34 ± 8% of the maximal Shh-driven response; $P < 0.01$), although activation was at a lower level than with the Trp535Leu variant (54 ± 12%) (Fig. 2a). Notably, overexpression of SMO Leu412Phe in immortalized mouse ameloblast-lineage cells (the ALC line[10]) enhanced cell proliferation in comparison to overexpression of wild-type SMO or empty vector control (Fig. 3), demonstrating a relevant phenotype in a germane cell type.

Next, we evaluated the response of the SMO Leu412Phe mutant to various pharmacological Hedgehog-pathway inhibitors (Fig. 2b), including the SMO antagonists KAAD-cyclopamine

and vismodegib (Erivedge, Genentech), which bind the cyclopamine pocket of SMO, and itraconazole, which acts at the level of SMO but does not bind the cyclopamine pocket. KAAD-cyclopamine effectively inhibited the Leu412Phe mutant ($P < 1 \times 10^{-6}$), comparable to the Trp535Leu mutant, whereas an inhibitory effect was not observed for vismodegib. This difference in inhibition is likely due to a combination of the effect of the mutation on the binding pocket and the divergent chemical structures of the two compounds. Itraconazole was also found to be ineffective at inhibition; however, both SMO mutants were sensitive to ATO (also known as Trisenox, Teva) ($P < 1 \times 10^{-5}$), an inhibitor of downstream GLI effectors. For both SMO mutants, constitutive activity was also suppressed by supraphysiological overexpression of mouse Ptch1 in these $Smo^{-/-}$ MEFs (Supplementary Fig. 3). Interestingly, the Leu412 and Trp535 residues are both located within the SMO seven-transmembrane domain but map outside the crystallographically resolved binding pocket for small molecule cyclopamine mimics (Fig. 2c)[11]. These observations suggest that the p.Leu412Phe substitution, as with p.Trp535Leu, leads to constitutive SMO activation via similar allosteric effects on SMO conformation.

To further investigate the activity of the inhibitors, we sought to evaluate their efficacy in human ameloblastoma cell lines. Few such cell lines have been reported, but we found that the AM-1 line[12], derived from a mandibular tumor, harbored the *BRAF* mutation encoding p.Val600Glu but had no *SMO* mutation (Fig. 4a,b). Notably, AM-1 cells were sensitive to the BRAF inhibitor vemurafenib, with a half-maximal inhibitory concentration (IC_{50}) of 0.19 μM (Fig. 4c), within the range of IC_{50} values reported for vemurafenib-sensitive cell lines for melanoma (0.1–0.8 μM)[13] and colorectal cancer (0.025–0.35 μM)[14] harboring the BRAF p.Val600Gu alteration. These data support the potential efficacy of BRAF inhibitors in treating *BRAF*-mutant ameloblastomas.

Hedgehog and FGFR-MAPK pathway components are known to be expressed during tooth development and in ameloblastoma[15–17]. In particular, analyses using gene expression microarrays, immunohistochemistry and quantitative RT-PCR (qRT-PCR) have demonstrated differential expression of Hedgehog pathway genes in ameloblastoma[16,17]. While this manuscript was under preparation, Kurppa *et al.*[18], using targeted Sanger sequencing, reported *BRAF* mutations encoding p.Val600Glu in 63% (15/24) of ameloblastomas (all mandibular), consistent with our findings. Nonetheless, to our knowledge, our study is the first to identify a common mutation of the Hedgehog pathway component *SMO* and to functionally characterize the mutant SMO Leu412Phe protein. Our study is also the first, to our knowledge, to distinguish two molecular subclasses of ameloblastoma (*SMO* versus *BRAF* mutated) with different histological and odontological features that are potentially responsive to different molecularly targeted therapies, either established or in clinical trials.

Our findings highlight the relationship between ontogenesis and oncogenesis, in particular, with respect to the biology of epidermal placodes, which are miniorgans that generate both teeth and hair[11,15,16]. The Hedgehog and FGFR-MAPK pathways are essential for both tooth and hair genesis, and their expression patterns are quite similar. Both SHH and FGFR are expressed at the tip of the invaginating hair bud[19,20] and at the tip of the tooth invagination[15]. In both structures, loss of SHH signaling leads to stunted growth and

morphogenesis but does not prevent differentiation: enamel and dentin secretion occur in the tooth, and hair keratins are synthesized in the hair follicle. As with the genesis of their normal counterparts, both ameloblastoma and basal cell carcinoma have mutations in the Hedgehog pathway. We found that nearly half of our ameloblastomas had activating *SMO* mutations. Likewise, basal cell carcinomas, which are derived from the hair follicle, harbor mutations in *PTCH1* (30–40%) and *SMO* (6–13%), and nevoid basal cell carcinoma syndrome (or Gorlin syndrome) is defined by germline inactivating *PTCH1* mutations[21]. Interestingly, some individuals with Gorlin syndrome also develop keratocystic odontogenic tumors, distinct from ameloblastomas but underscoring the role of Hedgehog signaling in odontogenic neoplasms.

Also notable was the observed relationship between anatomical site and driver mutation, with ameloblastomas arising in the maxilla predominantly carrying *SMO* mutations and those occurring in the mandible mainly harboring *BRAF* mutations. This finding may reflect distinctive odontogenic pathways in the upper and lower dentition[3]. More broadly, this result underscores an emerging appreciation of the anatomical specificity of driver mutations, with this specificity presumably reflecting distinctive developmental pathways based on spatial, temporal and/or cell type–specific cues. Other recently identified examples include meningiomas, in which *NF2*-mutant tumors originate from lateral and posterior regions along the skull base, whereas tumors with wild-type *NF2* (including those with *SMO* mutation) originate from anterior and medial regions[8], and high-grade astrocytomas, in which *H3F3A* mutations encoding p.Lys27Met (in histone H3.3) characterize brainstem and thalamic tumors, whereas *H3F3A* mutations encoding p.Gly34Arg or p.Gly34Val and *IDH1* or *IDH2* mutations characterize cortical tumors[22].

From a clinical perspective, tumors (for example, melanomas) with *BRAF* mutation encoding p.Val600Glu are already being treated with FDA-approved targeted therapies (vemurafenib). Our data suggest that such therapies may be immediately relevant for patients with ameloblastomas positive for *BRAF* mutation encoding p.Val600Glu. Drug discovery for Hedgehog-pathway inhibitors is also an active area of research; however, current Hedgehog-pathway inhibitors are effective only with inactivating mutations of *PTCH* as demonstrated by the resistance of SMO Trp535Leu to FDA-approved SMO inhibitors. Experimental trials are using ATO to treat advanced basal cell carcinomas and medulloblastomas with SMO-activating mutations[23,24]. Our findings suggest that determining the molecular subtype, characterized either by activating *SMO* or MAPK–pathway mutations, might provide an accurate biomarker test to guide molecularly targeted therapy in ameloblastoma.

In summary, this study demonstrates an emerging approach of transcriptome sequencing in formalin-fixed, paraffin-embedded samples to identify clinically actionable mutations in rare cancers and molecularly defines the majority of the instances of a tumor type that previously had no effective medical therapy. Our findings suggest an immediately actionable drug target (BRAF Val600Glu) and targets of experimental therapies (SMO) for the majority of ameloblastoma cases.

URLs

SIFT, http://sift.jcvi.org/www/SIFT_enst_submit.html; Sequence Read Archive (SRA), http://www.ncbi.nlm.nih.gov/sra/; deFuse, http://compbio.bccrc.ca/; Chimerascan, https://code.google.com/p/chimerascan/; Primer3web, http://primer3.wi.mit.edu/.

ONLINE METHODS

Samples

Paraffin blocks from 28 cases of ameloblastoma were collected from the Departments of Pathology at Stanford University Hospital, the Cleveland Clinic, Oregon Health and Sciences University and the University of British Columbia, with Health Insurance Portability and Accountability Act (HIPAA)-compliant Stanford University Medical Center Institutional Review Board approval. Tissue sections stained with hematoxylin and eosin were reviewed by pathologists R.B.W. and R.T.S. Tumors were morphologically classified by R.B.W. and R.T.S. as plexiform, follicular or desmoplastic[25]. If a tumor of mixed morphology had a plexiform component, it was counted as plexiform. BRAF Val600Glu expression was evaluated by immunohistochemistry, using a Val600Glu-specific antibody (VE1, Ventana; 12 μg/ml) and peroxidase-based chromogenic staining (EnVision, Dako).

RNA sequencing library preparation and sequencing

Paired-end transcriptome sequencing (RNA-seq) was performed using sequencing libraries prepared from rRNA-depleted RNA isolated from archival formalin-fixed, paraffin-embedded ameloblastoma samples. In brief, tumor cores were sectioned (thickness of 10 μm), RNA was isolated using the AllPrep RNA/DNA FFPE kit (Qiagen) and RNA quality was verified by Bioanalyzer (Agilent Technologies). Sequencing libraries (insert size of 150 bp) were then prepared from 100 ng of rRNA-depleted RNA[26] using TruSeq RNA Sample Preparation Kit v2 (Illumina), with four indexed libraries loaded per flow-cell lane. Paired-end 75-bp sequencing was carried out on a HiSeq 2000 instrument (Illumina). The two ameloblastoma libraries yielded 101 and 277 million uniquely mapped reads.

Sequence analysis

For SNV analysis, FASTQ reads were uniquely mapped to hg19 using Bowtie 2 and TopHat 2 (refs. 27,28), and duplicate mapping reads were removed with Picard. SNVs were called with SNVMix2 (ref. 29) and further filtered and annotated with ANNOVAR (SIFT < 0.05)[30]. High-interest mutations had high driver prediction scores in Cravat and Chasm[31] and/or were confirmed to be somatic and reported more than once in the Catalogue of Somatic Mutations in Cancer (COSMIC). Gene mutations selected for validation included the high-interest mutations that were present in both samples and/or involved a gene or pathway that had been implicated in tissue-specific proliferation, differentiation or neoplasia. Analysis for fusion transcripts was performed with SnowShoes[32], deFuse[33] and Chimerascan[34].

Targeted-capture deep sequencing

Genomic DNA was extracted from paraffin-embedded tumor sections with the QIAamp DNA FFPE Tissue kit (Qiagen). DNA (500 ng) was then sequenced using a multiplexed targeted resequencing assay including 48 genes in relevant cancer-associated loci (TruSeq Amplicon Cancer panel, Illumina). Sequencing was carried out to an average depth of 1,000-fold on an Illumina MiSeq next-generation DNA sequencer. Variants were identified by the Illumina variant caller and further analyzed by filtering out common variants and polymorphisms. All mutations were confirmed bidirectionally. The assay had the sensitivity to detect a 1% mutation allele frequency in a wild-type background.

PCR and Sanger sequencing

Genomic DNA was isolated using the QIAamp DNA FFPE Tissue kit (Qiagen). Hot-start PCR using AmpliTaq Gold polymerase (Applied Biosystems) was performed in two rounds (with either the same or nested primer pairs), respectively, for 30 and 20 cycles (94 °C for 30 s, 54 °C for 30 s and 72 °C for 45 s). Sequencing primers were designed using Primer3 (ref. 35) and were vetted using SNPCheck 3. See Supplementary Table 2 for primer sequences. PCR products were verified by gel electrophoresis and purified with the QIAquick PCR Purification kit (Qiagen), and Sanger sequencing (Quintara Biosciences) was then performed. Sequence reads were examined by BLAST alignment to RefSeq transcripts and by manual review of the sequence traces.

SMO functional assays

Human *SMO* cDNA was obtained from Origene Technologies (clone SC122724). Constructs encoding wild-type, Leu412Phe and Trp535Leu SMO were PCR amplified and inserted into the pGEN expression vector using one-step isothermal DNA assembly as previously described[36]; all constructs were verified by automated DNA sequencing. 4C20 $Smo^{-/-}$ MEFs were used for signaling assays as previously described[12]. Briefly, $Smo^{-/-}$ cells were transfected with a plasmid DNA mixture composed of 2% (w/w) *SMO* (with or without 10% (w/w) Ptch1 cDNA) along with a mixture of 8×Gli-driven luciferase and SV40-driven *Renilla* luciferase reporter plasmids; a GFP expression plasmid was included to normalize the amount of transfected DNA in each well. Upon reaching confluence, cells were shifted to DMEM with 0.5% serum containing ShhN-conditioned medium, agonists or antagonists (or appropriate vehicle controls) where indicated and incubated for 48 h, at which point, luciferase activity was measured. ShhN-conditioned medium was collected from HEK293-ShhN cells as previously described[12] and diluted 20-fold (Fig. 2a,b) or 4-fold (Supplementary Fig. 1) for cell treatment. Cells were tested and confirmed to be negative for mycoplasma. Vismodegib was purchased from LC Laboratories. KAAD-cyclopamine was purchased from Toronto Research. Itraconazole was purchased from Sigma. Clinical-grade, pH-buffered ATO solution was a generous gift from M. Monje (Stanford University School of Medicine). All data points represent means ± s.d. (n = 3 wells per condition) and are representative of multiple independent experiments. For ameloblast-lineage cell experiments, ALC cells[10] were grown in DMEM with 10% FBS. The above constructs encoding Myc-tagged SMO were subcloned into pLentiCMV-Blast (Addgene), and the viruses generated were transduced into ALC cells; stably transduced cell pools (with

approximately 1×10^5 independent integrations) were selected in 40 μg/ml blasticidin for 7 d. SMO expression was verified by protein blotting using an antibody to the Myc tag (Cell Signaling Technology, 2276; 1:1,000 dilution). Cells were then plated (30,000 cells per well of a 6-well plate; in triplicate), and relative cell proliferation was determined by WST-1 assay after 24, 48 and 72 h. Data shown are representative of multiple independent experiments.

BRAF inhibitor studies

AM-1 cells[12] were grown in KSFM complete medium (Life Technologies), and COLO205 and COLO320 cells were grown in RPMI medium with 10% FBS. Cells were not tested for mycoplasma. BRAF Val600Glu protein expression was evaluated using a Val600Glu-specific antibody (NewEast Biosciences, 26039; 1:1,000 dilution). We plated 30,000–50,000 cells per well of a 6-well plate in triplicate, and vemurafenib (Santa Cruz Biotechnology) was added at the indicated concentrations or cells received vehicle control (1% DMSO). Cell viability was measured after 3–5 d by WST-1 assay. IC_{50} values were determined by fitting a nonlinear log (inhibitor) versus response curve using GraphPad Prism. Data shown are representative of multiple independent experiments.

Supplementary Material

Refer to Web version on PubMed Central for supplementary material.

Acknowledgments

We would like to thank E. Epstein for assistance. We would like to thank C. Millward, H. Kaplan and M. Labusch for histology and pathology support.

We are also grateful to H. Harada (Iwate Medical University) for sharing the AM-1 cell line.

References

1. Gorlin RJ, et al. Odontogenic tumors. Classification, histopathology, and clinical behavior in man and domesticated animals. Cancer. 1961; 14:73–101. [PubMed: 13707265]
2. Sweeney RT, et al. Desktop transcriptome sequencing from archival tissue to identify clinically relevant translocations. Am J Surg Pathol. 2013; 37:796–803. [PubMed: 23598961]
3. Tucker A, et al. The cutting-edge of mammalian development; how the embryo makes teeth. Nat Rev Genet. 2004; 5:499–508. [PubMed: 15211352]
4. Davies H, et al. Mutations of the *BRAF* gene in human cancer. Nature. 2002; 417:949–954. [PubMed: 12068308]
5. Parada LF, et al. Cooperation between gene encoding p53 tumour antigen and ras in cellular transformation. Nature. 1984; 312:649–651. [PubMed: 6390217]
6. Li Y, et al. Activation of FGF receptors by mutations in the transmembrane domain. Oncogene. 1997; 14:1397–1406. [PubMed: 9136983]
7. Xie J, et al. Activating *Smoothened* mutations in sporadic basal-cell carcinoma. Nature. 1998; 391:90–92. [PubMed: 9422511]
8. Clark VE, et al. Genomic analysis of non-*NF2* meningiomas reveals mutations in *TRAF7*, *KLF4*, *AKT1*, and *SMO*. Science. 2013; 339:1077–1080. [PubMed: 23348505]
9. Taipale J, et al. Effects of oncogenic mutations in *Smoothened* and *Patched* can be reversed by cyclopamine. Nature. 2000; 406:1005–1009. [PubMed: 10984056]

10. Nakata A, et al. Establishment and characterization of a spontaneously immortalized mouse ameloblast-lineage cell line. Biochem Biophys Res Commun. 2003; 308:834–839. [PubMed: 12927794]
11. Wang C, et al. Structure of the human smoothened receptor bound to an antitumour agent. Nature. 2013; 497:338–343. [PubMed: 23636324]
12. Harada H, et al. Establishment of ameloblastoma cell line, AM-1. J Oral Pathol Med. 1998; 27:207–212. [PubMed: 9682983]
13. Søndergaard JN, et al. Differential sensitivity of melanoma cell lines with *BRAF*^{V600E} mutation to the specific Raf inhibitor PLX4032. J Transl Med. 2010; 8:39. [PubMed: 20406486]
14. Yang H, et al. Antitumor activity of BRAF inhibitor vemurafenib in preclinical models of BRAF-mutant colorectal cancer. Cancer Res. 2012; 72:779–789. [PubMed: 22180495]
15. Dassule HR, et al. Sonic hedgehog regulates growth and morphogenesis of the tooth. Development. 2000; 127:4775–4785. [PubMed: 11044393]
16. Kumamoto H, et al. Expression of Sonic hedgehog (SHH) signaling molecules in ameloblastomas. J Oral Pathol Med. 2004; 33:185–190. [PubMed: 15128061]
17. Heikinheimo K, et al. Gene expression profiling of ameloblastoma and human tooth germ by means of a cDNA microarray. J Dent Res. 2002; 81:525–530. [PubMed: 12147741]
18. Kurppa KJ, et al. High frequency of BRAF V600E mutations in ameloblastoma. J Pathol. 2014; 232:492–498. [PubMed: 24374844]
19. Chiang C, et al. Essential role for Sonic hedgehog during hair follicle morphogenesis. Dev Biol. 1999; 205:1–9. [PubMed: 9882493]
20. Schneider MR, et al. The hair follicle as a dynamic miniorgan. Curr Biol. 2009; 19:R132–R142. [PubMed: 19211055]
21. Iwasaki JK, et al. The molecular genetics underlying basal cell carcinoma pathogenesis and links to targeted therapeutics. J Am Acad Dermatol. 2012; 66:e167–e178. [PubMed: 20800318]
22. Fontebasso AM, et al. Chromatin remodeling defects in pediatric and young adult glioblastoma: a tale of a variant histone 3 tail. Brain Pathol. 2013; 23:210–216. [PubMed: 23432647]
23. Kim J, et al. Arsenic antagonizes the Hedgehog pathway by preventing ciliary accumulation and reducing stability of the Gli2 transcriptional effector. Proc Natl Acad Sci USA. 2010; 107:13432–13437. [PubMed: 20624968]
24. Kim J, et al. Itraconazole and arsenic trioxide inhibit Hedgehog pathway activation and tumor growth associated with acquired resistance to smoothened antagonists. Cancer Cell. 2013; 23:23–34. [PubMed: 23291299]
25. Sciubba, JJ., et al. Atlas of Tumor Pathology. Vol. 29. Armed Forces Institute of Pathology; Washington, DC: 2001. p. 71-84.
26. Morlan JD, et al. Selective depletion of rRNA enables whole transcriptome profiling of archival fixed tissue. PLoS ONE. 2012; 7:e42882. [PubMed: 22900061]
27. Langmead B, et al. Fast gapped-read alignment with Bowtie 2. Nat Methods. 2012; 9:357–359. [PubMed: 22388286]
28. Kim D, et al. TopHat-Fusion: an algorithm for discovery of novel fusion transcripts. Genome Biol. 2011; 12:R72. [PubMed: 21835007]
29. Goya R, et al. SNVMix: predicting single nucleotide variants from next-generation sequencing of tumors. Bioinformatics. 2010; 26:730–736. [PubMed: 20130035]
30. Wang K, et al. ANNOVAR: functional annotation of genetic variants from high-throughput sequencing data. Nucleic Acids Res. 2010; 38:e164. [PubMed: 20601685]
31. Douville C, et al. CRAVAT: cancer-related analysis of variants toolkit. Bioinformatics. 2013; 29:647–648. [PubMed: 23325621]
32. Asmann YW, et al. A novel bioinformatics pipeline for identification and characterization of fusion transcripts in breast cancer and normal cell lines. Nucleic Acids Res. 2011; 39:e100. [PubMed: 21622959]
33. McPherson A, et al. deFuse: an algorithm for gene fusion discovery in tumor RNA-Seq data. PLoS Comput Biol. 2011; 7:e1001138. [PubMed: 21625565]

34. Iyer MK, et al. ChimeraScan: a tool for identifying chimeric transcription in sequencing data. Bioinformatics. 2011; 27:2903–2904. [PubMed: 21840877]

35. Untergasser A, et al. Primer3—new capabilities and interfaces. Nucleic Acids Res. 2012; 40:e115. [PubMed: 22730293]

36. Myers BR, et al. Hedgehog pathway modulation by multiple lipid binding sites on the smoothened effector of signal response. Dev Cell. 2013; 26:346–357. [PubMed: 23954590]

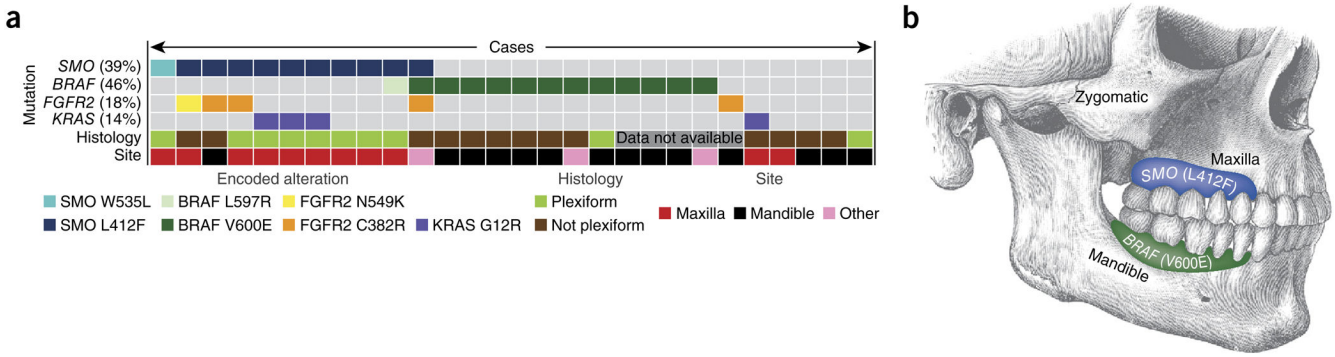

Figure 1.

Mutation frequency, distribution and relationship with pathological features. (**a**) Mutation status for four genes is indicated, and the overall percentage of mutant cases is given in parentheses. Information on histology and anatomical site is included below for each case. Each column represents a single case. Colors correspond to a specific mutation, histology or anatomical site. Details on additional clinical parameters are included in supplementary table 1. (**b**) Illustration of the distribution of tumors with the identified mutations.

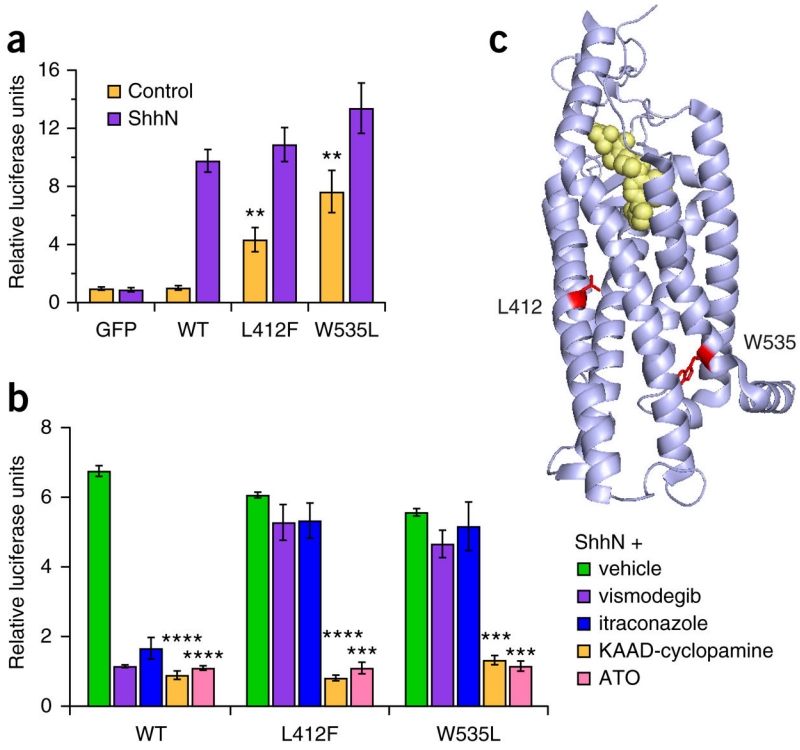

Figure 2.

SMO Leu412Phe activity and inhibition. (**a**) Relative expression of a Hedgehog-sensitive Gli-driven luciferase reporter in *Smo*$^{-/-}$ MEFs expressing GFP (negative control), wild-type human SMO (WT) or the Leu412Phe or Trp535Leu SMO mutants following stimulation with control medium or medium containing the Shh N-terminal domain (ShhN). Note the significant basal induction of Hedgehog-pathway activity by Leu412Phe and Trp535Leu. $^{**}P < 0.01$, two-sided Student's *t* test. Results are representative of five independent trials. (**b**) Effect of treatment with vismodegib (200 nM), itraconazole (2 μM), KAAD-cyclopamine (300 nM) and ATO (8 μM), showing significant reduction in Hedgehog activity in cells expressing SMO Leu412Phe and SMO Trp535Leu with KAAD-cyclopamine and ATO treatment. $^{***}P < 1 \times 10^{-5}$, $^{****}P < 1 \times 10^{-6}$, two-sided Student's t test. Results are representative of two independent trials. Data in **a**,**b** are from three independent transfections (three biological replicates), and error bars represent s.d. (**c**) Crystal structure of human SMO (Protein Data Bank (PDB) 4JKV) bound to the LY2940680 inhibitor[10] (yellow) with amino acids 412 and 535 highlighted (red) to show transmembrane domain positioning.

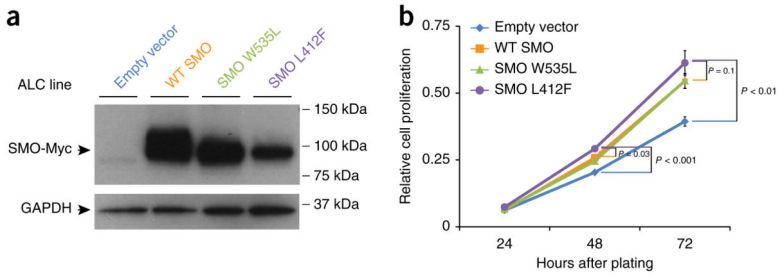

Figure 3.

SMO Leu412Phe enhances ameloblast-lineage cell proliferation. (**a**) Overexpression of wild-type SMO, SMO Trp535Leu, SMO Leu412Phe or empty vector control in mouse ameloblast-lineage (ALC) cells, shown by protein blot (antibody to Myc tag). GAPDH serves as a loading control. (**b**) Relative cell proliferation (in optical density (OD) units) evaluated by WST-1 assay (Roche) 24, 48 and 72 h after plating equal numbers of cells. Overexpression of SMO constructs significantly enhances cell proliferation compared to empty vector control; SMO Leu412Phe also enhances proliferation in comparison to wild-type SMO (two-sided Student's *t* test, *P* values indicated). SMO expression was engineered by lentiviral transduction, and stable cell pools (with approximately 1×10^5 independent integrations) were assayed. Cell proliferation was evaluated by three independent cell platings; error bars, s.d. Results presented are representative of three independent trials.

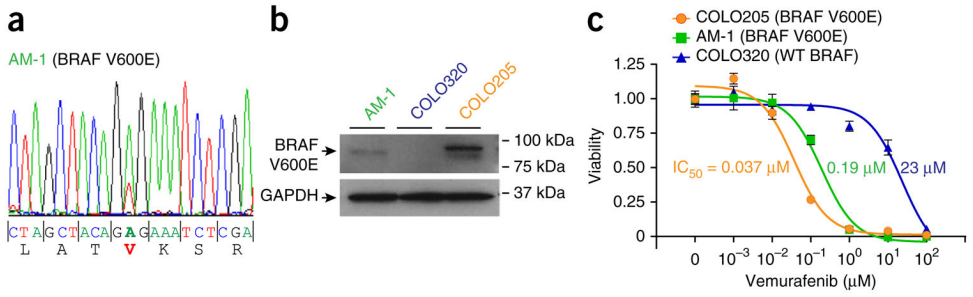

Figure 4.

An ameloblastoma cell line harboring BRAF p.Val600Glu is sensitive to the BRAF inhibitor vemurafenib. (**a**) PCR amplification with Sanger sequencing identifies a *BRAF* mutation encoding p.Val600Glu in the AM-1 ameloblastoma cell line. (**b**) Expression of RAF Val600Glu in AM-1 cells was confirmed by protein blot using Val600Glu-specific antibody. COLO320 (wild-type BRAF) and COLO205 (BRAF Val600Glu) colorectal cancer cell lines served as controls.

(**c**) Vemurafenib inhibits AM-1 cell proliferation/viability (fractional viability normalized to vehicle control) with an IC_{50} of 0.19 µM. Respective IC_{50} values for the control BRAF-mutant COLO205 and BRAF–wild type COLO320 cell lines are indicated. Data are representative of three independent cell platings; error bars, s.d. Results presented are representative of two independent trials.